PHYSICAL REVIEW D **87,** 114006 (2013)

Single top production in association with a Z boson at the LHC

John Campbell,* R. Keith Ellis,† and Raoul Röntsch‡
Fermilab, Batavia, Illinois 60510, USA
(Received 10 April 2013; published 5 June 2013)

We present results for the production of a Z boson in association with single top at next-to-leading order (NLO), including the decay of the top quark and the Z boson. This electroweak process gives rise to the trilepton signature $l^+l^-l'^{\pm}$ + jets + missing energy. We present results for this signature and show that the rate is competitive with the contribution of the mixed strong and electroweak production process, $t\bar{t}Z$. As such it should be observable in the full data sample from LHC running at $\sqrt{s} = 8$ TeV. The single top + Z process is a hitherto unconsidered irreducible background in searches for flavor changing neutral current decays of the top quark in $t\bar{t}$ production. For a selection of cuts used at the LHC involving a b-tag it is the dominant background. In the Appendices we also briefly discuss the impact of NLO corrections on the related tH process.

DOI: 10.1103/PhysRevD.87.114006 PACS numbers: 13.85.−t, 14.65.Ha, 14.70.Hp

I. INTRODUCTION

After only one year of 8 TeV running, the LHC has already become a tool for detailed studies of the top quark. With an increase to a higher centre-of-mass energy and anticipated integrated luminosities of up to 3000 fb^{-1}, the LHC will be able to achieve measurements of unprecedented precision in the top sector. With the advent of high statistics top physics, it will be possible to study not only the production of top quark pairs but also processes in which a vector boson is produced in association with top quarks.

The CMS and ATLAS collaborations have produced first results on $t\bar{t}Z$ and $t\bar{t}W$ production in recent publications [1,2]. The $t\bar{t}W$ process does not depend on the details of the top sector since the accompanying W boson is radiated from the initial state quarks. In contrast, the $t\bar{t}Z$ process directly probes the coupling of the Z boson to the top quark. Theoretical predictions are available for these processes at the NLO parton level [3–5] and in NLO calculations matched to a parton shower [6,7].

In this context it is also interesting to consider the process where an extra Z boson is radiated in t-channel single top production. This predominantly proceeds through the leading order processes,

$$u + b \to d + t + Z, \qquad \bar{d} + b \to \bar{u} + t + Z, \quad (1)$$

for the production of a top quark, with smaller contributions from strange- and charm-initiated reactions. Production of an anti-top quark proceeds through the charge conjugate processes,

$$d + \bar{b} \to u + \bar{t} + Z, \qquad \bar{u} + \bar{b} \to \bar{d} + \bar{t} + Z, \quad (2)$$

with a smaller rate at the LHC due to the difference in up- and down-quark parton distribution functions (pdfs). The leading order (LO) Feynman diagrams for the first process in Eq. (1) are shown in Fig. 1, including also the nonresonant contribution, diagram (g), that should be included when considering the charged lepton final state. The Z boson can be radiated from any of the four quark lines, or from the W boson exchanged in the t-channel. As can be seen from the diagrams, this process is related to hadronic WZ production by crossing. As a matter of principle, measurement of single top + Z is thus as important as measuring the WZ pair cross section, with the added bonus that it depends on the coupling of the top quark to the Z. In this paper, we present results for the single top + Z process to next-to-leading order (NLO) in QCD [8].

Although the single top + Z process is an electroweak one, in contrast to the QCD-induced pair production mode ($t\bar{t}Z$), it contains fewer particles in the final state and is therefore easier to produce. Figure 2 shows that any

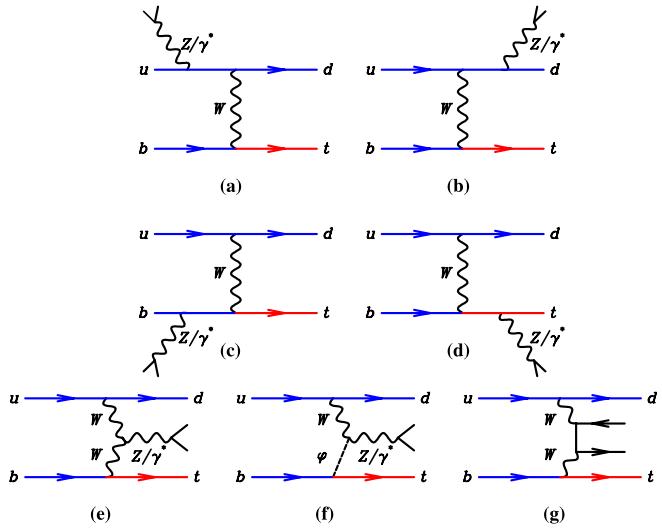

FIG. 1 (color online). Feynman graphs to calculate the lowest order amplitudes. The wavy line denotes a W or Z/γ^* boson. The Z boson may be emitted off one of the quark lines, as in (a)–(d), or off the t-channel exchanged W boson, as in (e) and (f). The nonresonant contribution is shown in (g).

*johnmc@fnal.gov
†ellis@fnal.gov
‡rontsch@fnal.gov

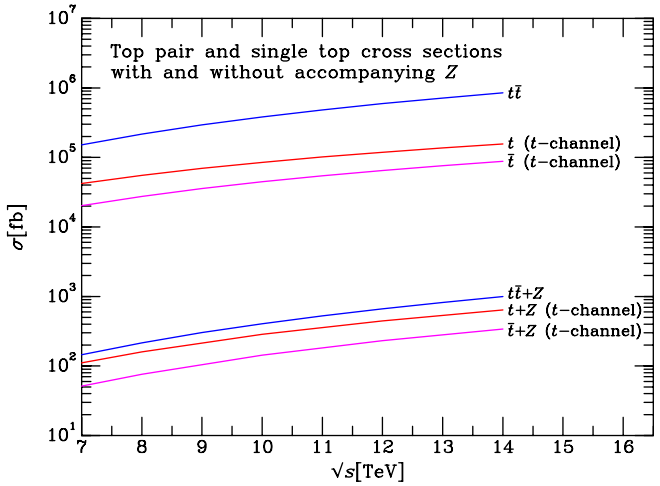

FIG. 2 (color online). NLO inclusive cross sections for single and top quark pair production with and without an accompanying Z boson. The NLO $t\bar{t}Z$ cross section is estimated from the lowest order result using a K-factor of 1.39 and renormalization and factorization scales $\mu = m_t + m_Z/2$ [4].

advantage in rate for the top pair production is effectively removed once an additional Z boson is required. As a result, the single top + Z cross section is about the same size as the $t\bar{t}Z$ one. Given the status of current LHC searches for $t\bar{t}V$ production it is interesting to consider the expected experimental sensitivity to the single top + Z channel. In particular, the impact of these SM processes should already be present in current trilepton searches, albeit in regions of lower jet multiplicity.

In order to properly assess the expected event rates in trilepton searches, in this paper we will consider the full process (and similarly for the charge conjugate process),

$$\begin{aligned} u + b \;\to\; & t + Z + d \\ & \quad\; \hookrightarrow \mu^- + \mu^+ \\ & \quad\; \hookrightarrow \nu + e^+ + b \end{aligned} \tag{3}$$

where the leptonic decay of the top quark is included and we have specified the charged leptons that are associated with the Z decay. The top quark decay is included using the techniques described in Refs. [10–12] and retains all spin correlations at the expense of requiring the top quark to be treated exactly on-shell. Since this calculation involves an incoming b-quark it is necessarily a five-flavor calculation.

We have also considered the closely-related single top + H process which is of smaller phenomenological interest in the standard model. A brief description of the next-to-leading order result is given in Appendix B.

II. OUTLINE OF CALCULATION

A. Leading order

The leading order diagrams for this process are shown in Fig. 1. It is useful to consider the contribution from combinations of individual diagrams as follows: the $Z/\gamma^\star$ attached to the light quark line, $M^{(a,b)}$, the $Z/\gamma^\star$ attached to the heavy quark line, $M^{(c,d)}$, the $Z/\gamma^\star$ attached to the t-channel W boson $M^{(e,f)}$, the nonresonant contribution with the lepton line attached to the t-channel exchanged W bosons, $M^{(g)}$. The computation of the amplitude can be performed in the unitary gauge. However, a more compact expression is obtained in the Feynman gauge after the inclusion of an additional contribution representing the propagation of unphysical Higgs fields [represented by φ in diagram (f)]. In the latter approach the cancellation of the terms associated with the longitudinal degrees of freedom is built-in. The explicit form of the leading order amplitudes is given in Appendix A.

B. Next-to-leading order

Next-to-leading order corrections to the single top + Z process are computed in a fairly straightforward manner. Virtual corrections to diagrams in which the Z boson is radiated from the t-channel W or in which the lepton pair are produced in a nonresonant manner [c.f. Figs. 1(e)–1(g)] consist solely of vertex corrections and are therefore easily computed analytically. For the remaining diagrams, where the Z boson is radiated from one of the fermion lines, some of the vertex corrections can be computed in a similar fashion. However, the virtual amplitude also receives contributions from box diagrams containing three powers of the loop momentum. These corrections are computed numerically using a variant of the van Oldenborgh-Vermaseren scheme for the calculation of tensor integrals [13]. Scalar integrals are computed using the QCDLoop library [14]. We have also implemented a version of the usual Passarino-Veltman reduction algorithm [15], supplemented by special handling of regions of small Gram or Cayley determinants according to the procedure outlined in Ref. [16]. In our implementation we find that the alternate reduction methods are used to improve the numerical stability of the calculation in approximately 0.3% of all events.

As a further numerical stability check, we compare the numerical calculation of the singular contributions to the amplitude to the known analytic form (after renormalization) [17],

$$\begin{aligned} g^2 c_\Gamma C_F \Bigg\{ & \left(\frac{\mu^2}{s_{16}}\right)^\epsilon \left[-\frac{2}{\epsilon^2} - \frac{3}{\epsilon} \right] + \left(\frac{\mu^2}{s_{25}}\right)^\epsilon \left[-\frac{2}{\epsilon^2} - \frac{5}{2\epsilon} \right] \\ & + \left(\frac{\mu^2}{m_t^2}\right)^\epsilon \left[\frac{1}{\epsilon^2} + \frac{3}{2\epsilon} \right] \Bigg\}. \end{aligned} \tag{4}$$

where the invariants s_{25} and s_{16} are taken from the momentum assignment in Eq. (A9). The overall factor c_Γ is,

$$c_\Gamma = \frac{1}{(4\pi)^{2-\epsilon}} \frac{\Gamma(1+\epsilon)\Gamma^2(1-\epsilon)}{\Gamma(1-2\epsilon)}. \tag{5}$$

We find that less than 0.02% of all events fail this consistency check and are discarded. Moreover, these points lie in extreme phase space regions that contribute little to total cross sections. When realistic experimental cuts are applied the proportion of numerically unstable points removed from the calculation drops by a factor of about four.

The calculation is performed in the four-dimensional helicity (FDH) scheme [18]. The mass renormalization is fixed by the condition that the inverse propagator vanish on-shell. In the FDH scheme we have

$$Z_m = 1 - c_\Gamma g^2 C_F \left[\frac{3}{\epsilon} + 3\ln\left(\frac{\mu^2}{m^2}\right) + 5\right] + \cdots, \quad (6)$$

and the wave function renormalization is

$$Z_Q = 1 - g^2 c_\Gamma C_F \left[\frac{3}{\epsilon} + 3\ln\left(\frac{\mu^2}{m^2}\right) + 5\right] + \cdots \quad (7)$$

The coupling of the scalar φ to the quark field, proportional to the top mass, must also be renormalized in the same way.

We have compared our results at the level of virtual matrix element squared with the results of the publicly available program GOSAM [19]. Additionally, we find excellent agreement when comparing the undecayed cross sections to AMC@NLO [20,21] at both LO and NLO.

The top quark decay is included using the method of Ref. [12]. We have included only the leading order amplitude for the decay since the rate for this process is already very small.

III. RESULTS

For the results that we present in this paper, we have used the parameters listed in Table I. From these, the Weinberg angle is fixed by the tree-level relation,

$$\sin^2\theta_W = 1 - \frac{m_W^2}{m_Z^2}, \quad (8)$$

which ensures that the amplitudes are gauge invariant. Since our calculation is performed in the five-flavor scheme, with an initial state massless b-quark, we also set $m_b = 0$ in the decay of the top quark. For simplicity we work in the framework of a unit CKM matrix. The parton distributions employed are the CTEQ6L1 set (used at LO) and CTEQ6M set (used at NLO) taken from Ref. [22]. The renormalization and factorization scales,

TABLE I. Input parameters used for the phenomenological results. The two values of $\alpha_S(m_Z)$ correspond to the choices made in the CTEQ6L1 and CTEQ6M pdf sets, used at LO and NLO respectively.

m_W	80.398 GeV	Γ_W	2.1054 GeV
m_Z	91.1876 GeV	Γ_Z	2.4952 GeV
m_t	173.2 GeV	G_F	1.116639×10^{-5}
$\alpha_S^{\mathrm{LO}}(m_Z)$	0.130	$\alpha_S^{\mathrm{NLO}}(m_Z)$	0.118

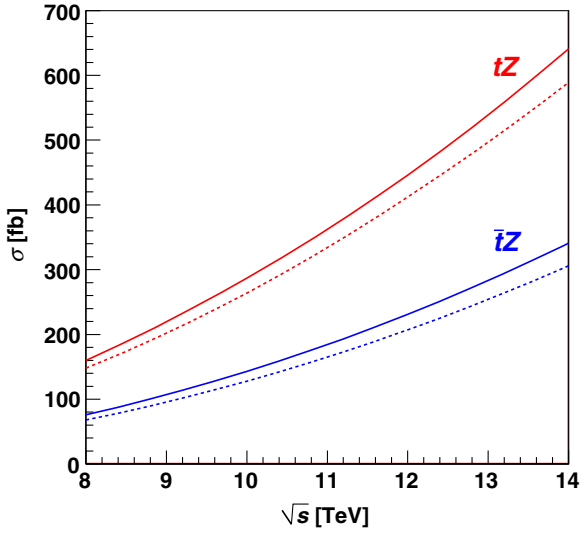

FIG. 3 (color online). Cross sections for tZ and $\bar{t}Z$ production as a function of $\sqrt{s}$. The leading order predictions are shown as dashed lines and the next-to-leading order solid lines.

denoted by μ_R and μ_F respectively, are taken to be the same for our standard scale choice, $\mu_R = \mu_F = m_t$.

With these parameters, the total cross sections for tZ and $\bar{t}Z$ production as a function of the LHC operating energy $\sqrt{s}$ are shown in Fig. 3. Although the leading order process contains a quark, the t-channel exchange of the W boson means that the amplitude does not contain a collinear singularity and thus that the inclusive cross section is well-defined. The cross section for $\bar{t}Z$ production is approximately half the corresponding tZ rate, a reflection of the corresponding parton distribution function ratio, $f_d(x)/f_u(x) \approx 0.5$ at values of x typical of those relevant for this process, $x \geq (m_t + m_Z)/\sqrt{s} \approx 0.02$–$0.03$. The NLO corrections take a similar form for both processes, resulting in an increase in the cross section predictions of the order of 10%. Finally, we see that although the cross sections are only of the order of a few hundred femtobarns at $\sqrt{s} = 8$ TeV, these processes have a combined cross section that is approximately a picobarn at $\sqrt{s} = 14$ TeV.

To investigate the scale dependence of this process we focus on the centre-of-mass energy $\sqrt{s} = 8$ TeV. Since the tree level process does not contain a strong coupling the resulting cross section only depends on the factorization scale, but at next-to-leading order the renormalization scale enters for the first time. We find that varying both scales together in the same direction leads to an accidental cancellation and therefore an artificially small estimate of the scale dependence. We therefore choose to vary them in opposite directions, $\mu_R = r m_t$, $\mu_F = m_t/r$ with $r \in [1/4, 4]$. We have checked that this variation reproduces the envelope of the extrema which would be obtained using the scale variation procedure of Ref. [23] with our range of r. The results are shown in Fig. 4, where one can see that the overall scale dependence is still very

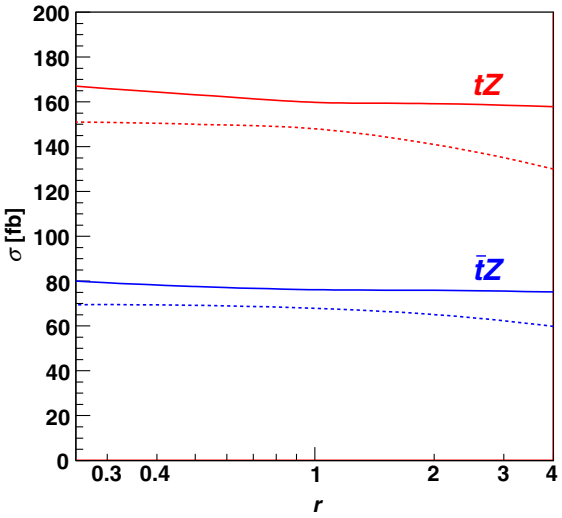

FIG. 4 (color online). Scale dependence of single top + Z cross sections at 8 TeV. The renormalization and factorization scales are varied in opposite directions according to $\mu_R = rm_t$, $\mu_F = m_t/r$.

weak. Even over such a large scale range the largest deviation from the central value is less than six percent.

Before turning to less inclusive cases, we summarize our findings by presenting predictions for LO and NLO cross sections at $\sqrt{s} = 8$ TeV. For the NLO prediction it is useful to consider the theoretical uncertainty that should be attributed to the calculation. In addition to the scale dependence uncertainty, based on the variation of r over the full range as described above, we also consider the effect of uncertainties in the extraction of the pdfs. By using the additional uncertainty sets provided in the CTEQ6 distribution, we find that this uncertainty is at the level of 7%. We thus find

$$\sigma_{\rm LO}(tZ) = 148 \text{ fb}, \qquad \sigma_{\rm NLO}(tZ) = 160^{+7}_{-2} \pm 11 \text{ fb},$$
$$\sigma_{\rm LO}(\bar{t}Z) = 68 \text{ fb}, \qquad \sigma_{\rm NLO}(\bar{t}Z) = 76^{+4}_{-1} \pm 5 \text{ fb},$$

where the first error shown is due to the scale variation, and the second due to the pdfs. Combining these, the single top + Z cross section is thus predicted with a total uncertainty of just over 10%.

A. Comparison of rates for tZ, $\bar{t}Z$ and $t\bar{t}Z$

As discussed in the introduction, the cross section for $t\bar{t}Z$ production is comparable to that for the sum of tZ and $\bar{t}Z$ production. Referring to Eq. (3), the signature for tZ production is three charged leptons, missing energy (which can be reconstructed up to the usual two-fold ambiguity) and jets. One of the jets may be b-tagged, although we ignore that possibility in this section. In the top-pair production scenario, the subsequent semi-leptonic decay of one top and the hadronic decay of the other, together with the leptonic decay of the Z boson, gives rise to the same signature of three charged leptons, missing energy and jets. If some of the jets go undetected, then the question arises as to whether it is possible to disentangle these two production processes.

In order to answer this question, we calculate jet-binned cross sections for four processes,

$$\begin{aligned}
&(a)\, t(\to \nu_e e^+ b)Z \\
&(b)\, \bar{t}(\to e^- \bar{\nu}_e \bar{b})Z, \\
&(c)\, t(\to \nu_e e^+ b)\bar{t}(\to q\bar{q}\,\bar{b})Z, \\
&(d)\, t(\to q\bar{q}b)\bar{t}(\to e^- \bar{\nu}_e \bar{b})Z,
\end{aligned} \tag{9}$$

with the decay $Z \to \mu^-\mu^+$ understood in each case. We perform our comparison at the $\sqrt{s} = 14$ TeV LHC. The scale $\mu = m_t$ is used for the tZ and $\bar{t}Z$ calculations, and $\mu = m_t + m_Z/2$ for $t\bar{t}Z$, following Refs. [3,4]. We will make use of three sets of kinematic cuts. The first, which we refer to as "standard cuts," requires that the momenta of the leptons, jets and missing energy are each greater than 20 GeV, and that the pseudorapidity of the leptons and jets are constrained by $|\eta_l| < 2.5$ and $|\eta_j| < 3.5$. We also require that the leptons originating from the Z boson have an invariant mass within 15 GeV of m_Z, and the leptons originating from the W boson have an invariant mass within 30 GeV of m_W. Jets are constructed with the anti-k$_t$ algorithm using $\Delta R = 0.4$. The second set of cuts require a more central jet, $|\eta_j| < 2.0$, but are otherwise the same. We shall refer to these cuts as "$|\eta_j| < 2.0$" cuts. The third set of cuts is identical to the standard cuts, but the jets are constructed using $\Delta R = 0.7$. This is referred to as the "$\Delta R = 0.7$" setup.

The comparisons are shown for the LO results in Fig. 5. The figures on the left are for processes (a) and (c), which result in a final state signature with two positively charged leptons; the right-hand figures show processes (b) and (d), for which the signature includes two negatively charged leptons. Of course, the results for the $t\bar{t}Z$ process are the same irrespective of which top decays hadronically, whereas the tZ cross sections are a factor of approximately two greater than those for $\bar{t}Z$, as indicated in Fig. 3. This feature suggests a way of distinguishing between the single top + Z and $t\bar{t}Z$ processes, by, for example, considering the asymmetry between $l^+l^-l'^+$ and $l^+l^-l'^-$ production. This method would rely on a stringent rejection of backgrounds, some of which would display a similar asymmetry.

The first row of Fig. 5 corresponds to the standard set of cuts. It is seen that most of the jets in tZ production are able to pass these cuts, so that the two-jet bin dominates the total cross section. By contrast, the $t\bar{t}Z$ process has a small cross section in the two-jet bin and a negligible contribution to the one-jet bin.

The effect of lowering the cut on the jet pseudorapidity to $|\eta_j| < 2.0$ is shown in the second row. Since one of the jets in tZ production is usually quite forward, with the other one central, it is unsurprising to see that the one-jet bin is

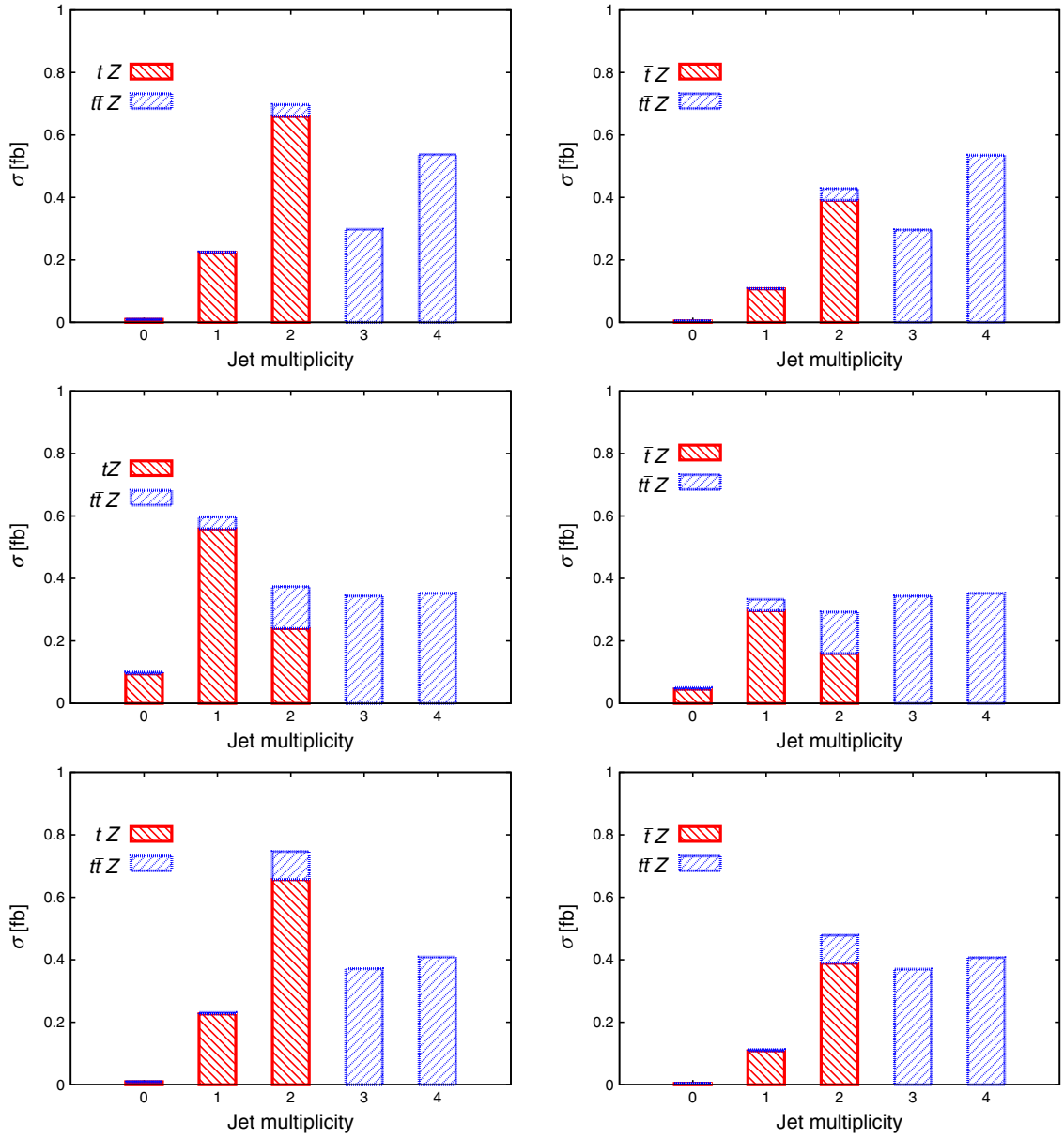

FIG. 5 (color online). Comparison of jet-binned cross sections calculated at LO at $\sqrt{s} = 14$ TeV. The left-hand plots show tZ production and $t\bar{t}Z$ production with the subsequent semi-leptonic decay of the top, resulting in a final state of $\mu^-\mu^+e^+$. The right-hand plots show $\bar{t}Z$ and $t\bar{t}Z$ production with the subsequent decay of the $\bar{t}$, with a final state of $\mu^-\mu^+e^-$. The first row corresponds to the standard cuts described in the text, the second row uses the $|\eta_j| < 2.0$ cuts, and the final row has the $\Delta R = 0.7$ setup. The scale $\mu = m_t$ is used for tZ and $\bar{t}Z$, and $\mu = m_t + m_Z/2$ is used for $t\bar{t}Z$.

dominant for tZ production. It is also evident that the stricter jet cut has shifted some of the $t\bar{t}Z$ events to the lower jet bins, with the result that the two-jet bin contains a significant proportion of events originating from this process.

The third row shows the results using the $\Delta R = 0.7$ setup. This has little effect on the jets originating from tZ production: since one is forward and the other one central, there is little opportunity for these to be clustered into one jet. The effect is more pronounced for $t\bar{t}Z$, enhancing the cross section in the two-jet bin.

The effect of NLO corrections to the $tZ + \bar{t}Z$ cross sections are shown in Table II. The total cross section shows a slight increase from $\sigma_{\mathrm{LO}} = 1.4$ fb at LO to $\sigma_{\mathrm{NLO}} = 1.5$ fb at NLO. However, looking at the standard cuts, it is clear that this increase is not uniform over the jet bins. The three-jet bin contributes around half the total cross section, indicating that the additional radiated gluon is usually quite hard. This has the effect of migrating events from one jet bin to the next, with the result that the cross sections in the zero-, one- and two-jet bins decrease due to the NLO corrections. This holds true when a larger jet is

TABLE II. Jet-binned LO and NLO cross sections (in fb) for $tZ + \bar{t}Z$ production at the $\sqrt{s} = 14$ TeV LHC, for the three sets of cuts described in the text.

Jet multiplicity		0	1	2	3
Standard cuts	LO	0.014	0.331	1.05	⋯
	NLO	0.011	0.237	0.585	0.693
$\lvert\eta_j\rvert < 2$	LO	0.140	0.856	0.400	⋯
	NLO	0.115	0.669	0.531	0.211
$\Delta R = 0.7$	LO	0.014	0.336	1.05	⋯
	NLO	0.010	0.241	0.661	0.614

used, $\Delta R = 0.7$, although the two-jet bin is larger and the three-jet bin smaller than with the standard cuts. This is because of the increased likelihood of clustering the radiated gluon with one of the LO partons, leaving two jets. When the $|\eta_j| < 2.0$ cuts are used, the NLO corrections decrease the one-jet bin and increase the two-jet bin. The three-jet bin is much smaller than for the standard set of cuts.

The NLO corrections indicate that distinguishing between tZ and $t\bar{t}Z$ production may be more difficult than a LO calculation leads one to expect. The NLO corrections deplete the tZ cross sections in the bins where they are dominant over the $t\bar{t}Z$ cross sections, and result in comparable cross sections in the three-jet bin, which only received contributions from $t\bar{t}Z$ at LO. Nor is this the final story. A more realistic calculation of the jet-binned cross sections would take parton showering into account. These effects can have a significant impact on exclusive observables. It should also be borne in mind that NLO corrections and/or parton showering effects may modify the $t\bar{t}Z$ results. Ideally, a comparison would be performed after calculating both processes to NLO in QCD, and then interfacing them with a parton showering program that preserves the NLO accuracy.

B. Single top + Z as a background in non-standard top decay searches

The top quark decays primarily via a W boson, $t \to Wq$, with a bottom quark being the most likely decay product and the presence of strange or down quarks suppressed by the off-diagonal CKM elements. In the standard model, decays through a flavor-changing neutral current (FCNC) are loop-suppressed, yielding a very small branching ratio $\mathcal{B}(t \to Zq) < 10^{-12}$ [24]. Therefore, the observation of such a decay would be indicative of new physics. Searches for FCNC decays in $t\bar{t}$ production were conducted by both CDF [25] and D0 [26]. Currently, the best constraints come from $t\bar{t}$ production at the LHC: ATLAS constrains the branching ratio $\mathcal{B}(t \to Zq) < 0.73\%$ with 2.1 fb^{-1} of data at $\sqrt{s} = 7$ TeV [27], while CMS constrains $\mathcal{B}(t \to Zq) < 0.24\%$ with 5.0 fb^{-1} of data at the same energy [28].

As the second top is taken to decay through the standard model mode $t \to Wb$, the signature of these events (with leptonic decays of both the W and Z bosons) is three charged leptons, missing energy from a neutrino (whose longitudinal momentum is reconstructible, up to the usual two-fold ambiguity), and two or more jets, one of which can be b-tagged. The same signature is expected in tZ and $\bar{t}Z$ production. However, neither the ATLAS [27] nor the CMS [28] analysis take this background into account. The purpose of this section is to look at the role of tZ and $\bar{t}Z$ production as a background to FCNC top decays.

We consider decays of the W and Z bosons into different flavored leptons, $Z \to \mu^-\mu^+$ and $W \to \nu_e e$, and impose a set of cuts similar to those used in the CMS analysis [29]:

(i) Leptons are required to have transverse momentum $p_{T,l} > 20$ GeV and pseudorapidity $|\eta_l| < 2.5$.
(ii) The missing transverse momentum is constrained by $p_{T,\text{miss}} > 30$ GeV.
(iii) Jets are defined with the anti-k_T algorithm with $\Delta R = 0.5$, and are required to have $p_{T,j} > 30$ GeV and $|\eta_j| < 2.4$, and to be separated from any lepton by $\Delta R_{jl} > 0.4$.
(iv) The same-flavor dilepton pair is required to have mass 60 GeV $< m_{ll} <$ 120 GeV. This pair is taken as originating from the Z boson, with the remaining lepton originating from the W boson.
(v) Each lepton is required to be isolated. In particular, the ratio of the sum of the transverse energies and momenta of all objects (leptons and jets) within $\Delta R = 0.3$ of the lepton to the lepton's transverse momentum must be less than 0.125 for leptons originating from the Z boson, and less than 0.1 for the lepton originating from the W boson:

$$\frac{\sum_{\Delta R_W < 0.3}(E_T + p_T)}{p_{T,l}} < 0.1;$$
$$\frac{\sum_{\Delta R_Z < 0.3}(E_T + p_T)}{p_{T,l}} < 0.125$$

(for our purposes, we set $E_T = p_T$).

In addition to the above cuts, CMS uses two further sets of cuts, called "S_T" cuts and "b-tag" cuts. In the case of the former, the following cuts are applied:

(i) At least two jets are required, with the transverse momentum cut as above.
(ii) The total transverse momentum $S_T = \sum_j p_{T,j} + \sum_l p_{T,l} + p_{T,\text{miss}} > 250$ GeV.
(iii) The masses of the Zj and Wb-system are constrained to be between 100 and 250 GeV.

The "b-tag" cuts are

(i) At least two jets are required, one of which is b-tagged.
(ii) The masses of the Zj- and Wb-systems are constrained to be close to the top mass: $|m_{Zj} - m_t| <$ 25 GeV and $|m_{Wb} - m_t| < 35$ GeV.

TABLE III. Leading- and next-to-leading order cross sections (in ab) for $Z(\to \mu^-\mu^+)t(\to \nu_e e b)j$ using the two classes of cuts used in the CMS searches for FCNC in top decays. The cross sections are evaluated at a scale $\mu = m_t$, with the integration error in the last digit in parentheses. The effect of using a scale choice of $\mu = m_t/2$ and $\mu = 2m_t$ are shown as subscripts and superscripts respectively.

		S_T cuts	b-tag cuts
Ztj	$\sigma_{\rm LO}$	$33.3(1)^{+1.2}_{-2.0}$	$14.3(1)^{+0.6}_{-0.8}$
	$\sigma_{\rm NLO}$	$52.0(1)^{-1.6}_{+2.8}$	$24.5(1)^{-0.9}_{+1.5}$
$Z\bar{t}j$	$\sigma_{\rm LO}$	$17.5(1)^{+0.6}_{-1.0}$	$7.71(1)^{+0.26}_{-0.46}$
	$\sigma_{\rm NLO}$	$26.2(1)^{-0.7}_{+1.1}$	$12.5(1)^{-0.4}_{+0.8}$

The LO and NLO cross sections for tZ and $\bar{t}Z$ production are shown at the $\sqrt{s} = 7$ TeV LHC in Table III. There is a negligible change when the three charged leptons have the same flavor. We note that the NLO corrections have a substantial effect on the cross sections, with a K-factor of around 1.5 for the S_T cuts and 1.7 when the b-tagging cuts are used. This is because the additional jet from the real radiation helps to satisfy the jet cuts. The scale uncertainty is larger than discussed previously for the inclusive production, and we estimate these uncertainties by varying both the factorization and renormalization scales in the same direction, between $m_t/2$ and $2m_t$. This gives a scale uncertainty of around 5%–7%. The pdf uncertainty is not taken into account, but is expected to be similar in magnitude.

The dominant background in the CMS analysis comes from $WZjj$ production, with leptonic decay of the weak bosons. Imposing the S_T cuts we calculate this cross section to be 0.91 fb at LO, with a scale uncertainty of around 25%. Multiplying by a factor of four to include all leptonic final states eee, $ee\mu$, $\mu\mu e$, $\mu\mu\mu$, we find in a sample of 5.0 fb^{-1} that this corresponds to $0.91 \times 4 \times 5 = 18.2$ events. This is consistent with the CMS calculation of 13.6 ± 2.6 $WZjj$ events.

We can convert the cross sections of Table III into event rates to compare with the CMS study in similar fashion. This implies that 1.6 events should be seen for the $tZ + \bar{t}Z$ background when the S_T cuts are used. This is a small but not negligible increase on the 16.2 overall background events that are expected. However, when the b-tag cuts are used, the overall CMS background estimation drops significantly to 0.83 events, due to a more stringent cut on the mass-window of the weak boson-jet system, and the requirement of a b-tag. Since our implementation of tZ production constrains the Wb-system to the top mass and guarantees the presence of a b-jet, the effect of these cuts is far less severe, and we expect 0.74 events coming from the $tZ + \bar{t}Z$ background with this set of cuts. At present, the best constraint on the FCNC branching ratio is found using the S_T cuts. However, it is possible that this situation could be changed once the dominant single top + Z contribution to the backgrounds with b-tag cuts is included.

IV. CONCLUSIONS

We have calculated the production cross section of single top + Z boson to NLO in QCD, including the leptonic decays of the top quark. We have demonstrated that this process is competitive in rate with the mixed strong and electroweak $t\bar{t}Z$ process. As such, it should be observable in recorded data from the LHC, despite being subject to a considerable reducible background from $W^{\pm}Z + 2$ jet processes. Given this, the potential to constrain the top-Z boson coupling through the tZ process should be investigated further. Moreover, we have shown that the use of jet-binned cross sections may be helpful in distinguishing this process from the $t\bar{t}Z$ process, although this requires further effort on the theoretical front to determine the effects of parton showering for this observable. In addition, this process constitutes an irreducible and potentially dominant background in searches for flavor changing neutral current decays in $t\bar{t}$ production, which is not taken into account in current searches. It will be challenging to remove because, like the signal, it contains a real top quark. Code for this phenomenological interesting process, as well as the related tH process, is included in MCFM v6.6.

ACKNOWLEDGMENTS

We gratefully acknowledge useful conversations with Kirill Melnikov and Giulia Zanderighi. We also thank the authors of Ref. [21] for bringing an error in an earlier version of this manuscript to our attention. This research is supported by the US DOE under Contract No. DE-AC02-06CH11357.

APPENDIX A: CALCULATIONAL DETAILS

1. Notation for spinor products

We adopt the following notation for massless spinors:

$$\begin{aligned} |i\rangle &= |i+\rangle = u_+(p_i), \qquad |i] = |i-\rangle = u_-(p_i), \\ \langle i| &= \langle i-| = \bar{u}_-(p_i), \qquad [i| = \langle i+| = \bar{u}_+(p_i). \end{aligned} \tag{A1}$$

Further the spinor products are defined as

$$\begin{aligned} \langle ij\rangle &= \langle i-|j+\rangle = \bar{u}_-(p_i)u_+(p_j), \\ [ij] &= \langle i+|j-\rangle = \bar{u}_+(p_i)u_-(p_j), \end{aligned} \tag{A2}$$

with p_i, p_j massless particles. With our convention,

$$\langle ij\rangle[ji] = 2p_i \cdot p_j = s_{ij}. \tag{A3}$$

We shall use the standard trick [30] of decomposing the massive momentum, $p^2 = m_t^2$ into the sum of two massless momenta, $p = p^\flat + \alpha\eta$ with the constant α given by

$$\alpha = \frac{m_t^2}{\langle\eta|\not{p}|\eta]}. \tag{A4}$$

We may write the massive spinors as combinations of massless spinors as follows:

$$\bar{u}_-(p) = [\eta|(\not{p} + m_t)\frac{1}{[\eta p^\flat]}, \tag{A5}$$

$$\bar{u}_+(p) = \langle \eta_t|(\not{p} + m_t)\frac{1}{\langle \eta_t p^\flat\rangle}, \tag{A6}$$

$$v_+(p) = (\not{p} - m_t)|\eta\rangle\frac{1}{\langle p^\flat \eta\rangle}, \tag{A7}$$

$$v_-(p) = (\not{p} - m_t)|\eta]\frac{1}{[p^\flat \eta]}. \tag{A8}$$

The spin labels of the massless spinors $|\eta\rangle$, $|\eta]$ encode the polarization information of the massive quarks and they are equivalent to helicities only in the massless limit.

2. Lowest order matrix element

We present results for the basic amplitude at leading order,

$$u(p_1) + b(p_2) \to l(p_3) + a(p_4) + t(p_5) + d(p_6), \tag{A9}$$

where l, a are the lepton and anti-lepton respectively and momentum labels for the particles are given in parentheses.

We begin by introducing the relevant couplings that appear in the calculation. The current for the emission of a Z boson or virtual photon that decays into a left-handed lepton pair enters with a strength,

$$\begin{aligned} V_j^L &= Q_j q_e + L_j l_e s_{34} D_Z(s_{34}), \\ V_j^R &= Q_j q_e + R_j l_e s_{34} D_Z(s_{34}), \end{aligned} \tag{A10}$$

where the superscript denotes the helicity of the outgoing quark and the subscript the flavor of the quark from which the boson is emitted ($j = u, d$). In this formula the individual quark and lepton couplings are themselves defined by

$$L_j = \frac{\tau_j - 2Q_j \sin^2\theta_W}{\sin 2\theta_W}, \qquad R_j = \frac{-2Q_j \sin^2\theta_W}{\sin 2\theta_W}, \tag{A11}$$

$$l_e = \frac{-1 - 2q_e \sin^2\theta_W}{\sin 2\theta_W}, \qquad r_e = \frac{-2q_e \sin^2\theta_W}{\sin 2\theta_W}, \tag{A12}$$

where $q_e = -1$, $\tau_u = 1$ and $\tau_d = -1$. The Z propagator denominator is

$$D_Z(s_{34}) = \frac{1}{s_{34} - m_Z^2}. \tag{A13}$$

We first consider the case of a negative helicity outgoing lepton and a negative spin-label for the top quark. The contributions to the amplitudes, calculated in the Feynman gauge and labelled by the diagrams in Fig. 1 are

$$\begin{aligned} &M^{(a,b)}(1_u^-, 2_b^-, 3_l^-, 4_a^+, 5_t^-, 6_d^+) \\ &\quad = D_W(s_{25})\frac{1}{s_{34}}\Big[\frac{V_u^L}{s_{134}}\langle 5^\flat\, 6\rangle[1\,4]\langle 3|1+4|2] \\ &\qquad - \frac{V_d^L}{s_{346}}\langle 3\,6\rangle[1\,2]\langle 5^\flat|3+6|4]\Big] \end{aligned} \tag{A14}$$

$$\begin{aligned} &M^{(c,d)}(1_u^-, 2_b^-, 3_l^-, 4_a^+, 5_t^-, 6_d^+) \\ &\quad = \frac{D_W(s_{16})}{s_{34}}\Big[-\frac{V_u^R m_t^2}{(s_{345} - m_t^2)}\frac{\langle 3\,6\rangle[1\,2][4\,\eta]}{[5^\flat\,\eta]} \\ &\qquad + \frac{V_d^L}{s_{234}}\langle 3|(2+4)|1]\langle 6\,5^\flat\rangle[2\,4] \\ &\qquad - \frac{V_u^L}{(s_{345} - m_t^2)}\langle 6|(1+2)|4]\langle 3\,5^\flat\rangle[1\,2]\Big] \end{aligned} \tag{A15}$$

$$\begin{aligned} &M^{(e,f)}(1_u^-, 2_b^-, 3_l^-, 4_a^+, 5_t^-, 6_d^+) \\ &\quad = \frac{D_W(s_{25})D_W(s_{16})}{s_{34}}\Big[-(V_u^L - V_d^L)\{\langle 3|(1+6)|4]\langle 6\,5^\flat\rangle[1\,2] \\ &\qquad + \langle 5^\flat|(1+6)|2]\langle 3\,6\rangle[1\,4] + \langle 6|(3+4)|1]\langle 3\,5^\flat\rangle[2\,4]\} \\ &\qquad + \frac{m_t^2}{2}\frac{\langle 3\,6\rangle[1\,4][2\,\eta]}{[5^\flat\,\eta]}\{V_u^L - V_d^L - V_u^R + V_d^R\}\Big] \end{aligned} \tag{A16}$$

$$\begin{aligned} &M^{(g)}(1_u^-, 2_b^-, 3_l^-, 4_a^+, 5_t^-, 6_d^+) \\ &\quad = \frac{D_W(s_{25})D_W(s_{16})}{2\sin^2\theta_W s_{235}}[\langle 3\,5^\flat\rangle[1\,4]\langle 6|(1+4)|2]]. \end{aligned} \tag{A17}$$

For the case of a positive spin-label for the top quark we have

$$\begin{aligned} &M^{(a,b)}(1_u^-, 2_b^-, 3_l^-, 4_a^+, 5_t^+, 6_d^+) \\ &\quad = D_W(s_{25})\frac{m_t}{s_{34}}\Big[\frac{V_u^L}{s_{134}}\frac{\langle 6\,\eta\rangle[1\,4]}{\langle 5^\flat\,\eta\rangle}\langle 3|(1+4)|2] \\ &\qquad + \frac{V_d^L}{s_{346}}\frac{\langle 3\,6\rangle[1\,2]}{\langle 5^\flat\,\eta\rangle}\langle \eta|(3+6)|4]\Big] \end{aligned} \tag{A18}$$

$$\begin{aligned} &M^{(c,d)}(1_u^-, 2_b^-, 3_l^-, 4_a^+, 5_t^+, 6_d^+) \\ &\quad = \frac{D_W(s_{16})m_t}{s_{34}}\Big[\frac{V_u^R}{(s_{345} - m_t^2)}\langle 3\,6\rangle[1\,2][4\,5^\flat] \\ &\qquad - \frac{V_d^L}{s_{234}}\frac{\langle 3|(2+4)|1]\langle 6\eta\rangle[2\,4]}{\langle 5^\flat\,\eta\rangle} \\ &\qquad + \frac{V_u^L}{(s_{345} - m_t^2)}\frac{\langle 6|(1+2)|4]\langle 3\,\eta\rangle[1\,2]}{\langle 5^\flat\,\eta\rangle}\Big] \end{aligned} \tag{A19}$$

$$M^{(e,f)}(1_u^-, 2_b^-, 3_l^-, 4_a^+, 5_t^+, 6_d^+)$$
$$= D_W(s_{25})D_W(s_{16})\frac{m_t}{s_{34}}\Big[(V_u^L - V_d^L)$$
$$\times\Big\{\frac{1}{\langle 5^\flat\,\eta\rangle}(\langle 3|(1+6)|4]\langle 6\,\eta\rangle[1\,2]$$
$$+\langle\eta|(1+6)|2]\langle 3\,6\rangle[1\,4] + \langle 6|(3+4)|1]\langle 3\,\eta\rangle[2\,4]\Big\}$$
$$+\frac{1}{2}\langle 3\,6\rangle[1\,4][2\,5^\flat]\{V_u^L - V_d^L + V_u^R - V_d^R\}\Big] \quad \text{(A20)}$$

$$M^{(g)}(1_u^-, 2_b^-, 3_l^-, 4_a^+, 5_t^+, 6_d^+)$$
$$= -\frac{D_W(s_{25})D_W(s_{16})m_t}{2\sin^2\theta_W s_{235}}\Big[\frac{\langle 3\,\eta\rangle[1\,4]\langle 6|(1+4)|2]}{\langle 5^\flat\,\eta\rangle}\Big]. \quad \text{(A21)}$$

Note that the opposite helicity combination for the lepton line is obtained by performing the flip $3 \leftrightarrow 4$, $l_e \to r_e$ for $M^{(a,b)}$, $M^{(c,d)}$, $M^{(e,f)}$. The amplitude $M^{(g)}$ does not contribute for the opposite helicity.

The total leading order amplitude is obtained by summing these four subamplitudes. In order to allow the Z boson to be off-shell but still retain gauge invariance, we use a simple prescription to incorporate the Z width [31]. We use the propagator factor $D_Z(s_{34})$ in the amplitudes as written above and then multiply the whole amplitude by

$$\left(\frac{s_{34} - m_Z^2}{s_{34} - m_Z^2 + im_Z\Gamma_Z}\right). \quad \text{(A22)}$$

An alternative prescription that also retains gauge invariance is the complex mass scheme [32]. We have calculated the leading order process using this scheme to assess the difference with our prescription. In the mass range $40\ \text{GeV} < \sqrt{s_{34}} < 140\ \text{GeV}$ the difference is at most 0.2%, a level much smaller than the scale uncertainty on the calculation.

APPENDIX B: ASSOCIATED PRODUCTION OF A SINGLE TOP AND HIGGS BOSON

In this appendix we briefly describe the NLO calculation of single top + Higgs boson production, which is very similar in many respects to the single top + Z process that is the main topic of this paper. In the limit in which the light quarks are taken to be massless, there are only two leading order diagrams, as shown in Fig. 6, with the Higgs boson attaching to either the top quark or the t-channel W boson. This process has previously been considered in Refs. [33–35]. The gauge cancellation between the two diagrams in Fig. 6 results in a smaller cross section

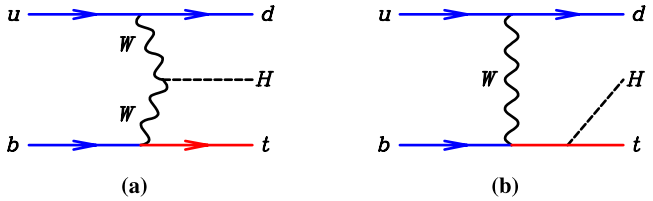

FIG. 6 (color online). Feynman graphs to calculate the lowest order amplitudes for single top + Higgs production. The diagrams where the Higgs boson couples to the light quarks have been dropped. The Higgs boson may be emitted from the exchanged W boson, as in (a), or from the top quark, as in (b).

compared to the associated pair production mode, $t\bar{t}H$. In addition, because of the small branching ratios of a 126 GeV Higgs boson to the cleanest modes ($H \to$ four leptons and $H \to \gamma\gamma$), single top + H production will be extremely challenging to observe. Nevertheless, like the $t\bar{t}H$ process, this channel has the potential to measure the coupling of the Higgs boson to the top quark. Reliable theoretical estimates for the $t\bar{t}H$ process, accurate to NLO, are given in Refs. [36–39] and including also the effect of a parton shower in Refs. [40,41]. Here we bring the accuracy of the single top + H channel to the NLO parton level.

Our results are calculated using the same numerical procedure described in Sec. II. Due to the simplicity of the scalar coupling of the Higgs, it is possible to immediately reduce the rank of the tensor integrals that appear in the 1-loop calculation to a maximum of two. As a result we find that the calculation is significantly more stable than the single top + Z case, with an order of magnitude less events discarded due to insufficient numerical precision in the pole terms (less than 0.005%). The renormalization of the Yukawa coupling of the Higgs boson to the top quark takes exactly the same form as the renormalization of the φ coupling already discussed in Sec. II. Again, we find excellent agreement when comparing our undecayed LO and NLO cross sections with those obtained from AMC@NLO [20,21].

For the results presented here we use $m_H = 126$ GeV based on the first observation of a new boson at the LHC. The cross sections for tH and $\bar{t}H$ production as a function of the LHC operating energy $\sqrt{s}$ are shown in Fig. 7 (left). The effect of next-to-leading order corrections is larger than in the single top + Z case, with an increase in the cross section of approximately 15% at NLO. To investigate the scale dependence of this process we focus on the case $\sqrt{s} = 8$ TeV. In contrast to the production of single top + Z, in this case we find the largest scale dependence when both renormalization and factorization scales are varied together. The results are shown in Fig. 7 (right), where we consider scale variation by a factor of four about the central value, $\mu = m_t$. Once again the NLO scale dependence is very mild, as expected in an electroweak process.

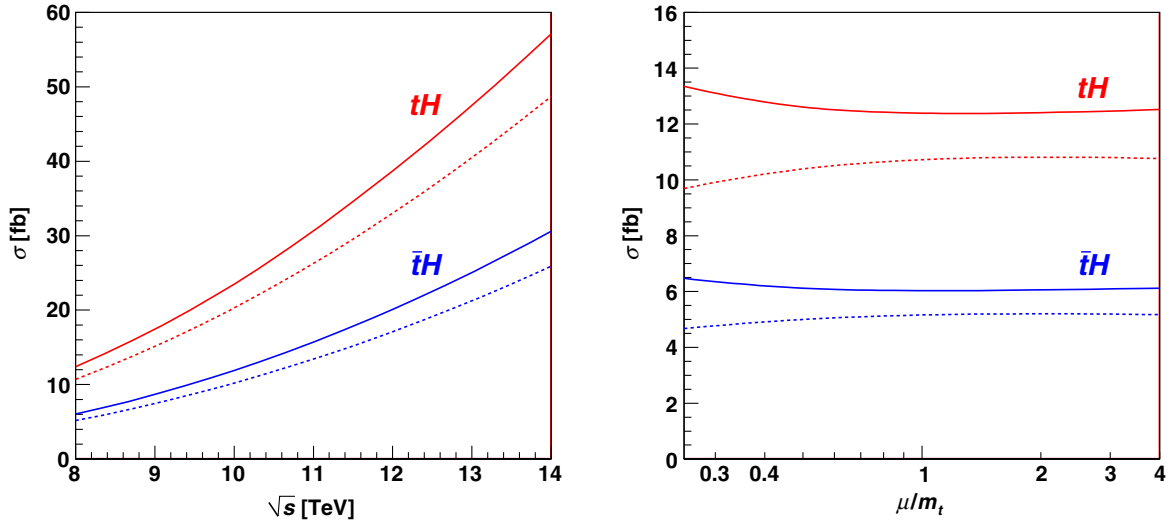

FIG. 7 (color online). Left: Cross sections for tH and $\bar{t}H$ production as a function of $\sqrt{s}$. Right: Scale dependence of single top + H cross sections at 8 TeV ($\mu = \mu_R = \mu_F$). In both cases, the Higgs boson has a mass $m_H = 126$ GeV and leading order predictions are shown as dashed lines, next-to-leading order as solid lines.

This process has received considerable interest recently as a probe of non-standard couplings of the Higgs boson to top quarks [35,42]. If the couplings deviate from their SM values (e.g. due to new physics effects in loops) then the tH cross section may be significantly enhanced. We allow the possibility of anomalous couplings in our code to enable a NLO calculation of such effects.

[1] CMS Collaboration, CERN Report No. CMS-PAS-TOP-12-014, 2012.
[2] ATLAS Collaboration, CERN Report No. ATLAS-CONF-2012-126, 2012.
[3] A. Lazopoulos, T. McElmurry, K. Melnikov, and F. Petriello, Phys. Lett. B **666**, 62 (2008).
[4] A. Kardos, Z. Trocsanyi, and C. Papadopoulos, Phys. Rev. D **85**, 054015 (2012).
[5] J. M. Campbell and R. K. Ellis, J. High Energy Phys. 07 (2012) 052.
[6] M. Garzelli, A. Kardos, C. Papadopoulos, and Z. Trocsanyi, Phys. Rev. D **85**, 074022 (2012).
[7] M. Garzelli, A. Kardos, C. Papadopoulos, and Z. Trocsanyi, J. High Energy Phys. 11 (2012) 056.
[8] Next-to-leading order QCD corrections to tZ associated production via the flavor-changing neutral-current couplings at hadron colliders have been considered in Ref. [9].
[9] B. H. Li, Y. Zhang, C. S. Li, J. Gao, and H. X. Zhu, Phys. Rev. D **83**, 114049 (2011).
[10] R. Kleiss and W. J. Stirling, Z. Phys. C **40**, 419 (1988).
[11] J. M. Campbell, R. K. Ellis, and F. Tramontano, Phys. Rev. D **70**, 094012 (2004).
[12] J. M. Campbell and R. K. Ellis, arXiv:1204.1513.
[13] G. van Oldenborgh and J. Vermaseren, Z. Phys. C **46**, 425 (1990).
[14] R. K. Ellis and G. Zanderighi, J. High Energy Phys. 02 (2008) 002.
[15] G. Passarino and M. J. G. Veltman, Nucl. Phys. **B160**, 151 (1979).
[16] A. Denner and S. Dittmaier, Nucl. Phys. **B734**, 62 (2006).
[17] S. Catani, S. Dittmaier, and Z. Trocsanyi, Phys. Lett. B **500**, 149 (2001).
[18] Z. Bern, A. De Freitas, L. J. Dixon, and H. Wong, Phys. Rev. D **66**, 085002 (2002).
[19] G. Cullen, N. Greiner, G. Heinrich, G. Luisoni, P. Mastrolia, G. Ossola, T. Reiter, and F. Tramontano, Eur. Phys. J. C **72**, 1889 (2012).
[20] R. Frederix, V. Hirschi, and F. Maltoni, private communication.
[21] V. Hirschi, R. Frederix, S. Frixione, M. V. Garzelli, F. Maltoni, and R. Pittau, J. High Energy Phys. 05 (2011) 044.
[22] J. Pumplin, D. R. Stump, J. Huston, H.-L. Lai, P. M. Nadolsky, and W.-K. Tung, J. High Energy Phys. 07 (2002) 012.
[23] T. Binoth, D. Gonçalves Netto, D. Lopez-Val, K. Mawatari, T. Plehn, and I. Wigmore, Phys. Rev. D **84**, 075005 (2011).
[24] E. N. Glover, F. del Aguila, J. Aguilar-Saavedra, M. Beccaria, S. Bejar *et al.*, Acta Phys. Pol. B **35**, 2671 (2004).
[25] T. Aaltonen *et al.* (CDF Collaboration), Phys. Rev. Lett. **101**, 192002 (2008).

[26] V. M. Abazov *et al.* (D0 Collaboration), Phys. Lett. B **701**, 313 (2011).
[27] G. Aad *et al.* (ATLAS Collaboration), J. High Energy Phys. 09 (2012) 139.
[28] S. Chatrchyan *et al.* (CMS Collaboration), Phys. Lett. B **718**, 1252 (2013).
[29] The cuts used by CMS are slightly more complicated, since they take into account various detector effects.
[30] R. Kleiss and W. Stirling, Nucl. Phys. **B262**, 235 (1985).
[31] U. Baur, J. Vermaseren, and D. Zeppenfeld, Nucl. Phys. **B375**, 3 (1992).
[32] A. Denner and S. Dittmaier, Nucl. Phys. B, Proc. Suppl. **160**, 22 (2006).
[33] F. Maltoni, K. Paul, T. Stelzer, and S. Willenbrock, Phys. Rev. D **64**, 094023 (2001).
[34] V. Barger, M. McCaskey, and G. Shaughnessy, Phys. Rev. D **81**, 034020 (2010).
[35] M. Farina, C. Grojean, F. Maltoni, E. Salvioni, and A. Thamm, J. High Energy Phys. 05 (2013) 022.
[36] W. Beenakker, S. Dittmaier, M. Krämer, B. Plümper, M. Spira, and P. Zerwas, Phys. Rev. Lett. **87**, 201805 (2001).
[37] L. Reina, S. Dawson, and D. Wackeroth, Phys. Rev. D **65**, 053017 (2002).
[38] W. Beenakker, S. Dittmaier, M. Krämer, B. Plümper, M. Spira, and P. M. Zerwas, Nucl. Phys. **B653**, 151 (2003).
[39] S. Dawson, C. Jackson, L. Orr, L. Reina, and D. Wackeroth, Phys. Rev. D **68**, 034022 (2003).
[40] M. Garzelli, A. Kardos, C. Papadopoulos, and Z. Trocsanyi, Europhys. Lett. **96**, 11001 (2011).
[41] R. Frederix, S. Frixione, V. Hirschi, F. Maltoni, R. Pittau, and P. Torrielli, Phys. Lett. B **701**, 427 (2011).
[42] S. Biswas, E. Gabrielli, and B. Mele, J. High Energy Phys. 01 (2013) 088.